University of Glasgow
DEPARTMENT OF
AEROSPACE
ENGINEERING

Implementation of a Vortex Method for the Prediction of Separated Incompressible Flows

H. Lin and M. Vezza

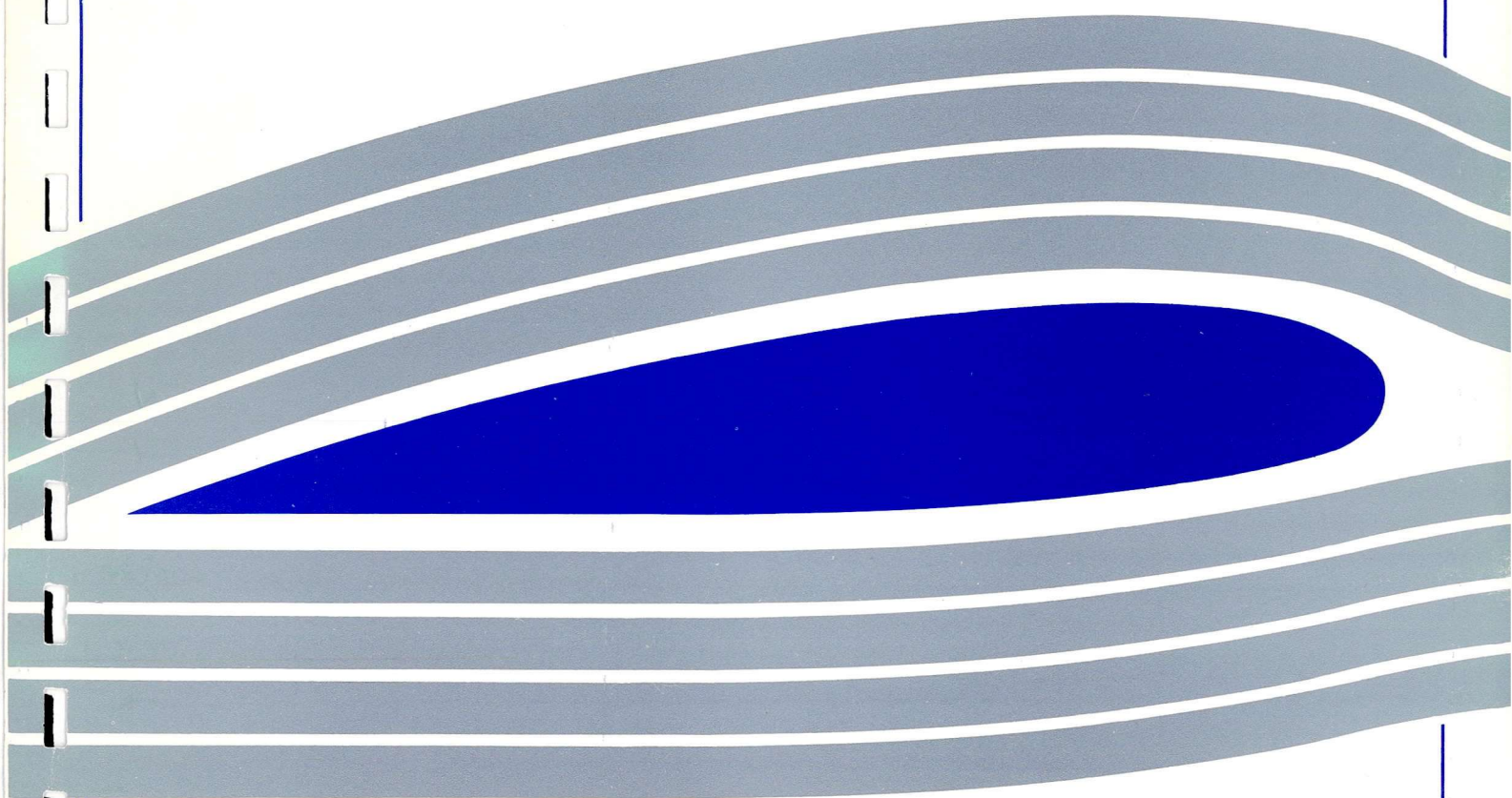

G.U. Aero Report No. 9425

Implementation of a Vortex Method for the Prediction of Separated Incompressible Flows

H. Lin and M. Vezza

Department of Aerospace Engineering
University of Glasgow
Glasgow G12 8QQ

November 1994

CONTENTS

NOMENCLATURE

A	Area of body (section)
F_b	Volume within the control zone
F_w	Volume outside the control zone
K	Total number of sub-panels for each panel
N	Number of panels for the body
P	Pressure
U,V	Velocity
Z	Position in the form of complex number
$\vec{\mathbf{k}}$	Unit vector
k	Index number of sub-panel within the panel
ℓ	length of panel
$\vec{\mathbf{n}}$	Unit vector normal to surface of body
$\mathbf{r}$	Position vector
r	Magnitude of position vector
$\vec{\mathbf{s}}$	Unit vector along the surface
t	Time
z	Position of vortices
Ω	Rotational velocity
Ψ	Stream function
Γ	Circulation
ρ	Fluid density
γ	Circulation density
υ	Kinematic viscosity
Δ	Distance of nascent vortex off the body
ω	Vorticity
σ	Vortex core radius

Subscripts

$_c$	Reference point for the body motion
$_f$	Free stream
$_i$	Index number for body
$_i$	Index number for vortices outside the control zone
$_i$	Equivalent vorticity inside the body
$_j$	Index number for panel
$_k$	Index number for sub-panel
$_m$	Index number for panel
$_m$	Moment
$_n$	Nascent vortices
$_n$	Normal force
$_s$	Surface velocity
$_t$	Tangential force
$_v$	Vortices outside the control zone
$_w$	Outside the control zone

Implementation of a Vortex Method for the Prediction of Separated Incompressible Flows

Summary

A vortex method has been developed to predict separated, incompressible flows around closed bodies. The method does not require any empirical data to model separation and employs random walks to simulate flow diffusion. The introduction of a control zone around the body results in realistic predictions for problems exhibiting different separation characteristics. Results of some cases are presented, including both a stationary and moving aerofoil in unsteady flow. The level of agreement between the results from the numerical model and tests is encouraging.

1 INTRODUCTION

As a technique to solve problems in incompressible fluid dynamics, the vortex method has undergone significant advances during last few decades. There are many vortex models which have been developed to simulate such flows - details can be found in comprehensive reviews [1][2]. The main features of the method are given below.

In the vortex method regions of flow vorticity are represented by a number of discrete vortex particles or vortices, which may or may not possess a finite viscous core. The time evolution of the system of vortices is calculated using the vorticity transport equation in conjunction with the Biot-Savart law, and the strength of the nascent boundary vorticity is evaluated by implementing appropriate boundary conditions on body surfaces. The vortices are tracked throughout the computation, therfore, in a Lagrangian manner and their total strength remains the same in most formulations.

In earlier formulations two of the main difficulties with the vortex method concerned the singularity of the velocity field in point vortex formulations, and the large amount of computing time required to implement the Biot-Savart calculations for n vortices ($O(n^2)$). Different core models, such as Rankine and Lame (Oseen) models, vortex blobs, and vortex balls were developed for tackling the singularity problem and to improve the convergence of the method. Reductions in computing time have been achieved by implementing faster interaction techniques e.g. cloud-in-cell, multipole expansions, and by reducing the number of vortices through absorption and merging.

The vortex method has been applied to a wide variety of both steady and unstaedy aerodynamic problems. Of particular interest to the Department of Aerospace Engineering is the vortex shedding which occurs during the dynamic stall of aerofoils. During the last fifteen years, several aerofoils have been tested under the unsteady aerodynamic conditions at the University of Glasgow and several papers have been published, summarised in [8] and [9]. Because of the presence of wind tunnel constraints in the experimental setup it is anticiptated that the algorithm presented herein for unrestricted external flow will be further developed to incorporate tunnel walls.

The theory behind the current method has been given in [6], and this paper concentrates primarily on the numerical implementation of the method. The main strength of the method lies in the treatment of the nascent vorticity near body surfaces, with the introduction of a buffer/absorption zone to eliminate spurious release of vortices, the implementation of integral boundary conditions, and inclusion of curvature effects in the linear panel representation. The resulting algorithm simulates the development of separated flows without the need to specify separation points, either empirically or via a boundary layer calculation, which is usually a requirement in vortex methods.

2 GOVERNING EQUATIONS

The governing equations for two dimensional incompressible flow are

continuity:

$$\nabla . \vec{\mathbf{U}} = 0 \tag{1}$$

momentum:

$$\frac{D\vec{\mathbf{U}}}{Dt} = -\frac{1}{\rho} \nabla P + \nu \nabla^2 \vec{\mathbf{U}} \tag{2}$$

solid region:

$$\vec{\mathbf{U}}_i = \vec{\mathbf{U}}_{ic} + \vec{\Omega}_i \times (\vec{\mathbf{r}} - \vec{\mathbf{r}}_{ic}) \tag{3}$$

boundary:

$$\vec{\mathbf{U}} = \vec{\mathbf{U}}_i \text{ on } S_i \text{ and } \vec{\mathbf{U}} = \vec{\mathbf{U}}_\infty \text{ on } S_\infty$$

By using the definitions of vorticity $\vec{\omega} = \nabla \times \vec{\mathbf{U}}$ with $\vec{\omega} = \vec{\mathbf{k}}\omega$, vector potential $\vec{\Psi}$ with $\vec{\mathbf{U}} = \nabla \times \vec{\Psi}$, $\vec{\Psi} = \vec{\mathbf{k}}\Psi$, $\nabla . \vec{\Psi} = 0$, and rotational velocity $\vec{\Omega}_i = \vec{\mathbf{k}}\Omega_i$, (1)-(3) can be expressed in vorticity/ stream function form

continuity:

$$\nabla^2 \Psi = -\omega \tag{4}$$

vorticity transport:

$$\frac{D\omega}{Dt} = \nu \nabla^2 \omega \tag{5}$$

solid region:

$$\nabla^2 \Psi_i = -2\Omega_i \tag{6}$$

boundary:

$$\nabla\Psi = \nabla\Psi_i \text{ on } S_i \text{ and } \nabla \Psi = \nabla\Psi_\infty \text{ on } S_\infty$$

The solution is given by

$$\begin{aligned} \vec{\mathbf{U}}_p &= \vec{\mathbf{U}}_\infty + \frac{1}{2\pi} \int_{F_b} \omega \frac{\vec{\mathbf{k}} \times (\vec{\mathbf{r}}_p - \vec{\mathbf{r}})}{\|\vec{\mathbf{r}}_p - \vec{\mathbf{r}}\|^2} dF_b + \frac{1}{2\pi} \int_{F_w} \omega \frac{\vec{\mathbf{k}} \times (\vec{\mathbf{r}}_p - \vec{\mathbf{r}})}{\|\vec{\mathbf{r}}_p - \vec{\mathbf{r}}\|^2} dF_w \\ &+ \frac{1}{2\pi} \int_{S_i} 2\Omega_i \frac{\vec{\mathbf{k}} \times (\vec{\mathbf{r}}_p - \vec{\mathbf{r}})}{\|\vec{\mathbf{r}}_p - \vec{\mathbf{r}}\|^2} dS_i \end{aligned} \tag{7}$$

where $F = F_b \cup F_w$ and $F_b \cap F_w = 0$.

The equation details the four contributions to velocity from; the free stream, the vorticity in the small control area around the solid region (control zone), the vorticity in the remaining flow area, and the vorticity inside the body due to the motion of the body.

The total circulation should remain the same according to Kelvin's Theorems. The total circulation generated by each individual body is

$$\Gamma_i = \int_{F_{bi}} \omega dF_{bi} + \int_{F_{wi}} \omega dF_{wi} + 2\Omega_i A_i = \text{constant} \tag{8}$$

The detailed description can be found in [6].

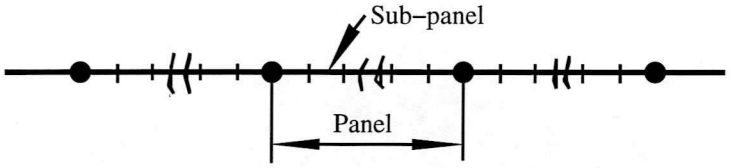

Figure 1: Schematic of the multi-panel discretisation

3 NUMERICAL IMPLEMENTATION

3.1 MULTI-PANEL REPRESENTATION OF BODY

For a two dimensional body, a polygonal representation of the body surface is created by connecting node points with a straight line to form a series of panels. The quality of the geometric approximation for curved surfaces improves as the number of node points increases and the length of the panel decreases.

Although the length of each panel can be defined arbitrarily, equal length provides the best consistency of solution. For example in the case of a two dimensional infinite plane sheet with constant circulation density, γ, placing a vortex at the centre of equal length panels satisfies the zero normal flow condition at each vortex location (and at each node point). Dividing one panel into two, however, destroys this agreement with the physical situation. The uniformly discretised surface therefore is superior in this respect.

For a body like an aerofoil, surface curvature is greatest near the leading edge, therefore a smaller panel length is required to obtain a more accurate representation. This increases the total number of panels for a model with uniform discretisation and as a result increases the computing time.

The discretisation process is illustrated in figure 1. N main node points are located on the body which define N plane panels approximating the N curved segments of the surface. Each curved segment is further subdivided into n equal length sub-panels by the specification of n-1 nodes along the segments. In areas of lower curvature the sub-panels are assumed to be colinear with the larger panels.

3.2 DISCRETISATION OF VORTICITY

The vorticity in the flow is discretised into vortices in the following way:

$$\omega(\vec{\mathbf{r}}) = \sum_k \delta_\sigma(\vec{\mathbf{r}} - \vec{\mathbf{r}}_k)\Gamma_k \tag{9}$$

where the core function δ_σ has integral 1, i.e. $\int_\infty \delta_\sigma(\vec{\mathbf{r}}-\vec{\mathbf{r}}_k)dV = 1$. There are many models for core functions such as Rankine, Rosenhead and Lame (Oseen) models. A very simple model [4] is presented here, with velocity distribution

$$V(r) = \frac{\Gamma}{2\pi}\frac{r}{r^2+\sigma^2} \tag{10}$$

and stream function

$$\Psi = \frac{\Gamma}{4\pi}\ln\left(r^2+\sigma^2\right) \tag{11}$$

where σ is the core radius.

The thin area near the body surface is regarded as a special zone, the control zone, in which the vorticity is created. The vorticity in the rest of the flow field arises through convection and diffusion of that generated in the control zone. The discretisation of vorticity in the control zone can be regarded as a two stage process.

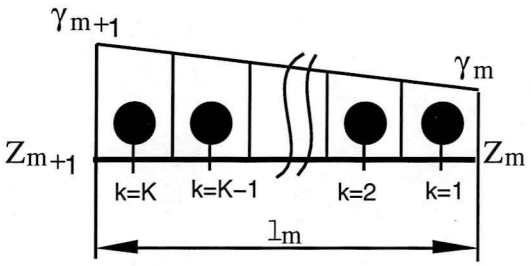

Figure 2: Discretisation and γ distribution

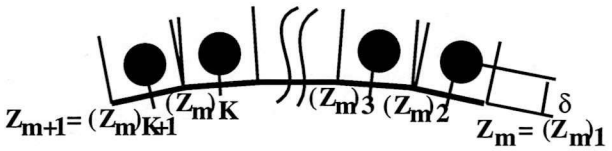

Figure 3: Schematic of discretisation for higher curvature panel

Firstly, the total vorticity normal to the surface within the control zone, γ, is treated as a quantity which varies piecewise linearly and continuously along the surface. The values of γ at main node points therfore represents the whole surface distribution.

Secondly, the panel distribution of total vorticity is further broken down into vortex blobs, one for each sub-panel. The blob is positioned a distance δ directly above the middle of the sub-panel . The discretisation is illustrated in figure 2

The vortex so generated is called a nascent vortex. It has circulation

$$(\Gamma_m)_k = \frac{\ell_m}{K}\left[\left(\frac{K-k+\frac{1}{2}}{K}\right)\gamma_m + \left(\frac{k-\frac{1}{2}}{K}\right)\gamma_{m+1}\right] \tag{12}$$

which is equivalent to the total vorticity in the control zone above the kth sub-panel, and can thus be related to the nodal values γ_m and γ_{m+1}. All of the nascent vortices can be related to the N nodal γ values for a body represented by N panels. The γ values are determined by implementing the boundary conditions.

The positioning of vortices in the surface regions with higher curvature, such as the leading edge of an aerofoil, is as shown in figure 3. $(z_m)_k$, the position of the nascent vortex above the kth sub-panel in panel m is given by:

$$(z_m)_k = \frac{1}{2}\left((Z_m)_{k+1} + (Z_m)_k\right) - i\frac{(Z_m)_{k+1} - (Z_m)_k}{|(Z_m)_{k+1} - (Z_m)_k|}\delta \tag{13}$$

In surface regions with lower curvature , such as the rear part of an aerofoil, the position can be approximated as:

$$(z_m)_k = \left[\left(\frac{K-k+\frac{1}{2}}{K}\right)Z_m + \left(\frac{k-\frac{1}{2}}{K}\right)Z_{m+1}\right] - i\frac{Z_{m+1} - Z_m}{|Z_{m+1} - Z_m|}\delta \tag{14}$$

which is equivalent to a straight panel with K vortices equally spaced over the panel as illustrated in figure 2

This distance between the nascent vortex and the body, δ, depends on the Reynolds number and the smoothness of the surface of the body.

3.3 BOUNDARY CONDITIONS AND SYSTEM EQUATIONS

The boundary condition, equation (3), is implemented by ensuring zero mass flow through each panel. Although this implementation cannot guarantee the equation (3) to be fullfilled at every point, there is at least one point on each panel with zero relative normal velocity. The implementation is expressed as

$$F_{js} + F_{ji} + F_{jf} + F_{jv} + F_{jn} = 0 \tag{15}$$

with each term representing the contribution of mass flow by different sources. The first and second terms are from the motion of the body and are thus additional items to those for the static case.

The contribution by the surface velocity of the body, to the panel with end points Z_j and Z_{j+1} is

$$F_{js} = \frac{1}{2}\Omega\left(|Z_{j+1} - Z_c|^2 - |Z_j - Z_c|^2\right) - \frac{i}{2}[V_c\overline{(Z_{j+1} - Z_j)} - \overline{V_c}(Z_{j+1} - Z_j)] \tag{16}$$

where the first term accounts for the rotation and the second for the translation.

The mass flow from the equivalent vorticity inside the body due to its rotation, 2Ω, is more complicated to calculate. The integral form is

$$F_{ji} = -\frac{\Omega_B}{2\pi}\int_0^{\ell_j}\left(\int_{S_B}\vec{\mathbf{s}}\ln|\vec{\mathbf{r}} - \vec{\mathbf{r}}_p|^2\, ds\right).\vec{\mathbf{n}}ds_j \tag{17}$$

Details of the integration are given in the Appendix.

The influence of the free stream can be written as

$$F_{jf} = \frac{i}{2}\left[V\left(\overline{Z_{j+1} - Z_j}\right) - \overline{V}\left(Z_{j+1} - Z_j\right)\right] \tag{18}$$

and the influence of the vortices outside the control zone can be expressed as

$$F_{jv} = -\sum_i \frac{\Gamma_i}{2\pi}\ln\frac{|Z_{j+1} - z_i|}{|Z_j - z_i|} \tag{19}$$

All vortices originate from nascent vortices. Their positions are the result of convection and diffusion at each time step. Their circulations are unchanged with time. At the beginning of the calculation, the total number of such vortices is zero, as is the mass flow contribution.

The final contribution to the mass flow is from the vorticity within the control zone, and takes the form

$$F_{jn} = -\sum_{m=1}^{N}\sum_{k=1}^{K}\frac{(\Gamma_m)_k}{2\pi}\ln\frac{|Z_{j+1} - (z_m)_k|}{|Z_j - (z_m)_k|} \tag{20}$$

The strength of the nascent vortices are obtained once the equations are solved for the N γ values.

The total number of equations (15) is N for a body with N panels, but only $N-1$ are independent because there is no source or sink within the body. Hence after $N-1$ panels satisfy zero mass flow, the mass flow for the final panel will automatically be zero.

A further equation required to make the solution unique is obtained from the Kelvin's theorem. The circulation of the vortices in the whole flow field remains constant because there is no external source of vorticity. For each body, the additional condition is

$$\sum_i \Gamma_i + \sum_{m=1}^{N}\sum_{k=1}^{K}(\Gamma_m)_k + \Gamma_{st} = 0 \tag{21}$$

where the first term is the circulation of vortices in the wake, the second is the circulation of the nascent vortices, and the third is the initial circulation in the flow field prior to the start of calculations. The second term contains the unknown γ values.

Combining equations (15) and (21), there are N equations for the N unknown γ values. The matrix form of the simultaneous equations is

$$\begin{bmatrix} a_{11} & \cdots & a_{1N} \\ \vdots & \ddots & \vdots \\ a_{N1} & \cdots & a_{NN} \end{bmatrix} \begin{Bmatrix} \gamma_1 \\ \vdots \\ \gamma_N \end{Bmatrix} = \{\mathbf{F}_s\} + \{\mathbf{F}_i\} + \{\mathbf{F}_v\} + \{\mathbf{F}_f\} \tag{22}$$

The elements of the square matrix are determined by the relative position of the panels and do not change with motion if there is only one solid body.

Other methods implement the boundary conditions differently, e.g. it is common to choose a specific point, known as the collocation point, where either the normal velocity or tangential velocity is set to zero. The point chosen may be the node point, the point at a quarter panel, half panel or three quarter panel position, and only one point is used for each panel. One of the problems for this implementation is that there may be one extra equation for the solution of circulation density after the implementation of the condition for total circulation. Other techniques, such as least squares, Lagrangian multiplier (λ) and ignoring one of the collocation points, are employed in some cases [1]. However these approaches can lead to fluid mass leaking through the body surface.

As described in section 3.2, sub-panels are used to discretise the vorticity near the surface while the plane panels between main nodes are for the implementation of the boundary conditions. The advantages of this model are that it can reduce computing time for calculations with a larger number of vortices, and it conveniently accounts for surfaces with high curvature. Generally, the more vortices used, the greater is the accuracy of the model. However, this is normally accompanied by more equations and hence higher computing times. The model presented here keeps the number of system equations smaller, by employing larger panels for implementing the boundary conditions, while increasing the accuracy of representing the body surface and nascent vorticity.

Usually, the distribution of vortices is directly connected to the discretisation of the body surface, but this is not actually a requirement. The main requirement is to ensure that the boundary condition is satified. The distinction in this model between discretising the vorticity and the representation of the body increases model flexibility.

3.4 CONVECTION AND DIFFUSION OF VORTICITY

The vorticity transport equation (5) can be rewritten

$$\frac{\partial \omega}{\partial t} + \left(\vec{\mathbf{U}}.\nabla\right)\omega = \nu \nabla^2 \omega \tag{23}$$

where the vorticity ω is a function of t, x, and y. The equation is nonlinear and direct solution is difficult. If considered as a two step process, convection followed by diffusion, the governing equations are

$$\frac{\partial \omega}{\partial t} + \left(\vec{\mathbf{U}}.\nabla\right)\omega = 0 \tag{24}$$

$$\frac{\partial \omega}{\partial t} = \nu \nabla^2 \omega \tag{25}$$

The convection equation (24) models vorticity transport in inviscid flow. The solution has been well documented. For point vortices, the velocity at each vortex location is the velocity of the vortex particle, and is given by

$$\vec{\mathbf{U}} = \vec{\mathbf{V}}_i + \vec{\mathbf{V}}_f + \vec{\mathbf{V}}_v + \vec{\mathbf{V}}_n \tag{26}$$

where the second term is for the free stream, the third for the contribution of the vortices in the wake and the fourth for the nascent vortices. The first term represents the influence of the equivalent vorticity inside the body due to its motion.

After time step Δt, every vortex progresses by one step. Its new position due to convection is

$$\left(z_i\left(t+\Delta t\right)\right)_c = z_i\left(t\right) + V_i\left(t\right)\cdot\Delta t \tag{27}$$

for nascent vortices, and

$$\left(z_i\left(t+\Delta t\right)\right)_c = z_i\left(t\right) + \left[\frac{3}{2}V_i\left(t\right) - \frac{1}{2}V_i\left(t-\Delta t\right)\right]\cdot\Delta t \tag{28}$$

for the vortices in the wake (Adams-Bashforth second order method).

For a unit vortex at the origin, the solution of the diffusion equation (25) after time Δt is

$$\omega = \frac{1}{4\pi\nu\Delta t}e^{-\frac{r^2}{4\nu\Delta t}} = \frac{1}{4\pi\nu\Delta t}e^{-\frac{\left(x^2+y^2\right)}{4\nu\Delta t}} \tag{29}$$

and is the vorticity to be found at position (x, y) at that moment. The vorticity is spread out as time increases. Discretising the vorticity within the square (x, y) to $(x+dx, y+dy)$ into a vortex, the strength is

$$\Gamma\left(\Delta t, x, y\right) = \frac{1}{4\pi\nu\Delta t}e^{-\frac{\left(x^2+y^2\right)}{4\nu\Delta t}}dxdy \tag{30}$$

Assuming two independent continuous random variables X and Y with the same normal distribution $(0, \sqrt{2\nu\Delta t})$, representing the coordinates of the position of a vortex at the origin undergoing a random walk during time period Δt, the joint density function of these two random variables is

$$f\left(x, y\right) = \frac{1}{4\pi\nu\Delta t}e^{-\frac{\left(x^2+y^2\right)}{4\nu\Delta t}} \tag{31}$$

which means the probability of finding a vortex in the square (x, y) to $(x+dx, y+dy)$ is

$$P\left(x, y\right) = f\left(x, y\right)dxdy = \frac{1}{4\pi\nu\Delta t}e^{-\frac{\left(x^2+y^2\right)}{4\nu\Delta t}}dxdy \tag{32}$$

Equally dividing a unit vortex into a large number of vortex elements, each of strength Γ_s, the total strength of vortex elements found within this square after each undergoes a random walk should be

$$\Gamma\left(\Delta t, x, y\right) = \sum\Gamma_s f\left(x, y\right)dxdy = \frac{1}{4\pi\nu\Delta t}e^{-\frac{\left(x^2+y^2\right)}{4\nu\Delta t}}dxdy \tag{33}$$

which is the same as the solution from the diffusion equation. The random walk model simulates the diffusion of vorticity in the overall flow field.

Suppose η_x, and η_y are two random numbers generated from the normal distribution $(0, \sqrt{2\nu\Delta t})$, then (η_x, η_y) would represent the position of a vortex due to the diffusion. Combining convection and diffusion, the vortex after time Δt will be at

$$\left(z_i\left(t+\Delta t\right)\right)_c = z_i\left(t\right) + V_i\left(t\right)\cdot\Delta t + \left(\eta_x, +i\eta_y\right) \tag{34}$$

for a nascent vortex and

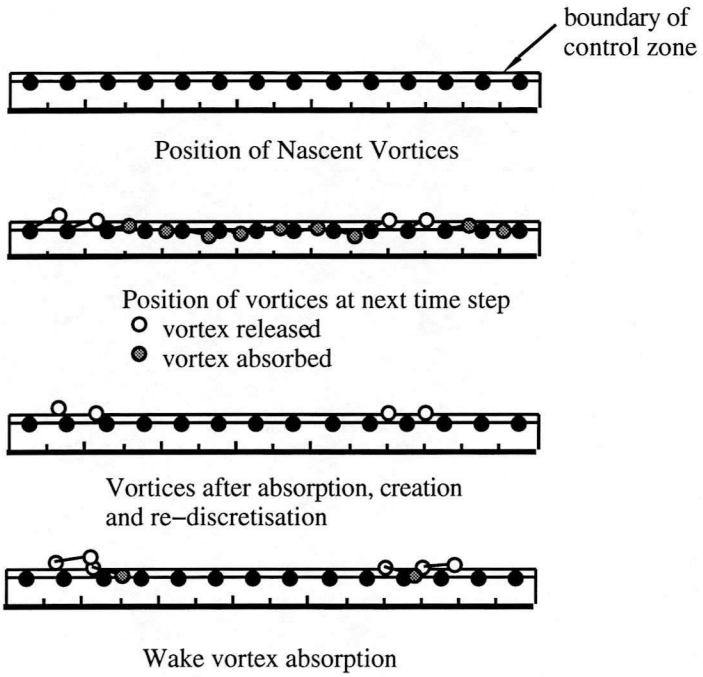

Figure 4: Illustration of vortex release and absorption

$$\left(z_i\left(t+\Delta t\right)\right)_c = z_i\left(t\right) + \left[\frac{3}{2}V_i\left(t\right) - \frac{1}{2}V_i\left(t-\Delta t\right)\right]\cdot\Delta t + \left(\eta_x + i\eta_y\right) \tag{35}$$

for the vortices outside the control zone.

3.5 RELEASE AND ABSORPTION OF VORTICES

Special treatment in the control zone is required to reduce the number of vortices in the field, and hence computing time, and to stabilise the implementation of the boundary conditions. A vortex is released into the wake, absorbed by the zone, or remains in the wake, depending on its relative position to the zone at the new time step. A nascent vortex from the previous step is said to be released if it crosses the control zone boundary, otherwise it is absorbed. Any vortex in the wake at the previous step is absorbed if it crosses into the control zone, otherwise it remains in the wake. This process is illustrated in the figure 4

The released vortices are treated as wake vortices, while those inside the zone are absorbed and replaced by nascent vortices, which also include the newly created vorticity, at the nascent vortex locations.

The normal velocity component of the vortices arises partly from the pressure distribution along the surface of the body, and partly from the effect of discretisation error on the stream function between main nodes. Zero mass flow through a panel ensures the correct stream function values at the main nodes (constant for a stationary body), but not at points in between. Figure 5 illustrates this for a typical panel, where the total mass flow is zero but this is achieved through a balance of outflow and inflow. To remove this non-physical effect on the velocity of the nascent vortices the border of the control zone is set above the position of these vortices, hence avoiding the common problem of premature vortex release.

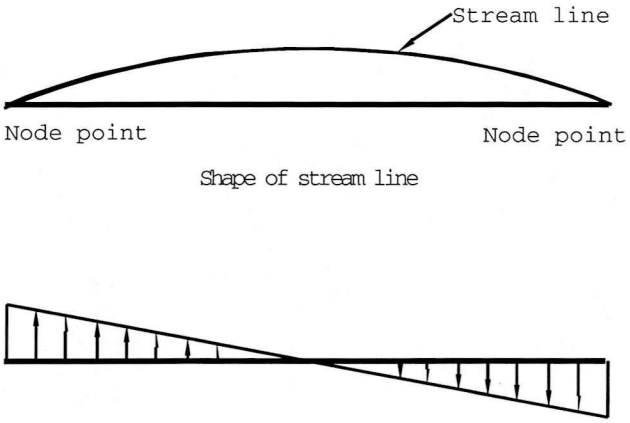

Figure 5: Schematic distribution of normal velocity

3.6 MERGING OF VORTICES

There are some vortices released from the control zone at each time step. The number of vortices in the wake increases steadily as the calculation progresses, as does the amount of computing time required. However vortices located far from a body will have less contribution to the boundary condition than those that are nearer. Hence vortices far from a body can be merged without influencing the result of solution significantly. A criterion[4] is used to decide if merging is allowed and this is described below.

Assuming two vortices at Z_1 and Z_2, with strengths Γ_1 and Γ_2 respectively, are merged into a vortex at Z with strength Γ according to the formula

$$\Gamma = \Gamma_1 + \Gamma_2 \tag{36}$$

$$Z = \frac{\Gamma_1 Z_1 + \Gamma_2 Z_2}{\Gamma_1 + \Gamma_2} \tag{37}$$

the difference between the induced velocity at Z from the original vortices and the merged vortex is

$$\begin{aligned} \Delta V &= \frac{i}{2\pi}\left[\frac{\Gamma_1\Gamma_2}{\Gamma_1+\Gamma_2}\cdot\frac{\left(\overline{Z}_1-\overline{Z}_2\right)^2}{\left(\overline{z}-\overline{z}_0\right)^3}\right. \\ &+ \left. O\left(\left|\frac{Z_1-z_0}{z-z0}\right|^4\right)+O\left(\left|\frac{Z_2-z_0}{z-z0}\right|^4\right)+O\left(\left|\frac{Z-z_0}{z-z0}\right|^4\right)\right] \end{aligned} \tag{38}$$

where z_0 is selected so that the last three terms can be neglected compared with the first term. Also the approximation

$$\begin{aligned} |z-z_0|^2 &= (D_0+d_1)(D_0+d_2) \\ d_1 &= |Z_1-z| \\ d_2 &= |Z_2-z| \end{aligned} \tag{39}$$

holds for specific D_0 when two vortices are close enough and far from point z.

Merging is allowed only if the velocity error at the point of interest is small enough. That is

$$\frac{|\Gamma_1\Gamma_2|}{|\Gamma_1+\Gamma_2|}\cdot\frac{|Z_1-Z_2|^2}{(D_0+d_1)^{1.5}(D_0+d_2)^{1.5}}\leq V_0 \tag{40}$$

In most circumstances the point of interest is on a body. If z is the point on a body nearest to Z_1 or Z_2 then d_1 and d_2 are the distances between them respectively.

From the above criterion vortices are more likely to be merged when they are closer, have less strength of the same sign, and are farther from the point of interest. This is also true for larger values of both the velocity tolerance V_0 and parameter D_0, the latter having a bigger influence the closer the vortices are to the point of interest.

Merging when criterion (40) is satisfied is not always appropriate. An example is an aerofoil where some of the vortices released near the leading edge will roll along the upper surface as part of a larger vortical structure. Vortices far from the body at a specific step may possibly approach the surface again after several time steps. Merging in this case would change the vortical structure over the body and hence significantly affect the flow field in this region.

One way of avoiding this situation arising is to tighten the criterion near a body and to loosen it in the far wake, where the structure is less important. This means choosing a different value of V_0 for the different regions, smaller for the area close to a surface, larger for the far wake.

3.7 PRESSURE DISTRIBUTION

Operating with $\vec{\mathbf{n}}\times$on the N-S equation (2) applied to a body surface, an equation for pressure gradient is obtained

$$\frac{1}{\rho}\frac{\partial P}{\partial s}=-\vec{\mathbf{s}}.\frac{D\vec{\mathbf{U}}}{Dt}+\nu\frac{\partial\omega}{\partial n} \tag{41}$$

where $\vec{\mathbf{n}}$, the normal vector, and $\vec{\mathbf{s}}$, the tangential vector are related by $\vec{\mathbf{n}}=\vec{\mathbf{s}}\times\vec{\mathbf{k}}$.

Because of the no-slip condition the flow velocity on the surface should be the same as that of the surface itself, given by (3). Hence (41) becomes (dropping index i)

$$\frac{1}{\rho}\frac{\partial P}{\partial s}=-\vec{\mathbf{s}}.\frac{D\vec{\mathbf{U}}_c}{Dt}-\vec{\mathbf{n}}.(\vec{\mathbf{r}}-\vec{\mathbf{r}}_c)\frac{D\Omega}{Dt}+\vec{\mathbf{s}}.(\vec{\mathbf{r}}-\vec{\mathbf{r}}_c)\Omega^2+\nu\frac{\partial\omega}{\partial n} \tag{42}$$

The first three terms on the right hand side of (42) only appear when the body is in motion and describe the surface tangential components of the acceleration of the reference point, the rotational acceleration and the centripetal acceleration. In the numerical calculation, time derivatives are approximated by

$$\begin{aligned}\frac{D\vec{\mathbf{U}}_c(t)}{Dt}&=\frac{\vec{\mathbf{U}}_c(t)-\vec{\mathbf{U}}_c(t-\Delta t)}{\Delta t}\\ \frac{D\Omega(t)}{Dt}&=\frac{\Omega(t)-\Omega(t-\Delta t)}{\Delta t}\end{aligned} \tag{43}$$

It is worth noting that $\vec{\mathbf{n}}$ and $\vec{\mathbf{s}}$ are time dependent for the dynamic case but $\vec{\mathbf{n}}.(\vec{\mathbf{r}}-\vec{\mathbf{r}}_c)$, $\vec{\mathbf{s}}.(\vec{\mathbf{r}}-\vec{\mathbf{r}}_c)$ are time independent.

The line integration of pressure gradient along the surface of a closed body should be zero because the pressure is a single value function. The only motion term which possesses a non-zero surface integral in (42) is the component due to rotational acceleration, and can be expressed as

$$\oint\vec{\mathbf{n}}.(\vec{\mathbf{r}}-\vec{\mathbf{r}}_c)\frac{D\Omega}{Dt}ds=-2A\frac{D\Omega}{Dt}=-2A\frac{\Omega(t)-\Omega(t-\Delta t)}{\Delta t} \tag{44}$$

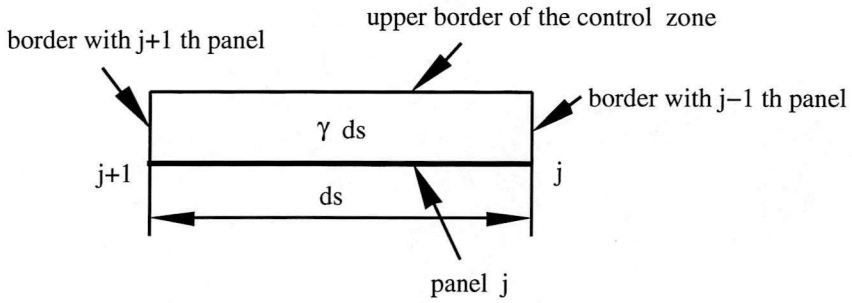

Figure 6: Vorticity inside the control zone

This is zero only if the rotational velocity is constant. Ramp-up or ramp-down motions are such cases, excluding any finite starting and finishing accelerations.

Rewriting the vorticity transport equation (5) as

$$\frac{D\omega}{Dt} = \frac{\partial \omega}{\partial t} + (\vec{\mathbf{u}}.\nabla)\,\omega = -\nabla\,.\,(-\nu\,\nabla\,\omega) \tag{45}$$

$\nu\nabla\omega$ is the vorticity flux which, when applied at the body, produces the surface flux $-\vec{\mathbf{n}}.\nu\nabla\omega = \nu\partial\omega/\partial n$. Therefore the last term in (42) can be regarded as the negative vorticity creation rate at the surface.

Consider a control area with one side on part of the body surface and the opposite side on the upper part of the control zone, figure 6. The control area has size ds along the surface and moves with the body. The circulation of vortices inside the control area at time t, excluding the vorticity created by the surface at this time, is $\gamma^a ds$. This includes the vorticity in existance there at time $t - \Delta t$ and the vorticity flux through the area boundaries (excluding the body surface) from $t - \Delta t$ to t. The circulation of vortices created at the element of surface during this time step is $(-\nu\partial\omega/\partial n)\,ds\Delta t$. The nett circulation of vortices inside this area, γds, is given by the sum of these contributions, that is

$$\left(-\nu\frac{\partial \omega}{\partial n}\right) ds\Delta t + \gamma^a ds = \gamma ds \tag{46}$$

so

$$\nu\frac{\partial \omega}{\partial n} = \frac{\gamma^a - \gamma}{\Delta t} \tag{47}$$

where γ^a is the equivalent circulation density of existing vortices in the control area at time t, and is approximated piecewise linearly in the same fashion as the nett vorticity γ.

To determine the distribution of the equivalent circulation density, $\{\gamma^a\}$, the contribution to the boundary condition of vortices within the control zone must be recorded, along with the total circulation of such vortices. This information is stored in vector $\{\mathbf{F}^a\}$. Discretising the equivalent vorticity into vortices at the nascent vortex positions allows the reuse of the system matrix

$$\begin{bmatrix} a_{11} & \cdots & a_{1N} \\ \vdots & \ddots & \vdots \\ a_{N1} & \cdots & a_{NN} \end{bmatrix} \begin{Bmatrix} \gamma_1^a \\ \vdots \\ \gamma_N^a \end{Bmatrix} = \{\mathbf{F}^a\} \tag{48}$$

This process effectively replaces the vortices within the control zone by nascent vortices producing the same effect on the mass flow through the surface. Total circulation is preserved from the condition

$$\oint \gamma^a\,(t)\,ds = \oint \gamma\,(t - \Delta t)\,ds - \Delta\Gamma\,(t) = -\Gamma_w\,(t) - 2A\Omega\,(t - \Delta t) \tag{49}$$

since for at each instant in time, the circulation should satisfy

$$\begin{aligned} \oint \gamma\left(t-\Delta t\right) ds &= -\Gamma_w\left(t-\Delta t\right) - 2A\Omega\left(t-\Delta t\right) \\ \oint \gamma\left(t\right) &= -\Gamma_w - 2A\Omega\left(t\right) \\ \Gamma_w\left(t\right) &= \Gamma_w\left(t-\Delta t\right) + \Delta\Gamma\left(t\right) \end{aligned} \tag{50}$$

where $\Delta\Gamma\left(t\right)$ is the nett circulation released from the control zone during the step from $t-\Delta t$ to t, and $\Gamma_w\left(t\right)$ is total nett circulation released from the body up to time t.

The line integration of (42) along the surface of the body produces, using (47),

$$\oint \nu \frac{\partial \omega}{\partial n} = \frac{1}{\Delta t} \oint \left(\gamma^a - \gamma\right) ds = 2A \frac{\Omega\left(t\right) - \Omega\left(t-\Delta t\right)}{\Delta t} \tag{51}$$

which is consistent with conditions (49) and (50), hence pressure closure is assured. Note also that there is no nett circulation generated from a surface when the rotational acceleration is zero.

For cases in which motion exists, care should be exercised where sudden changes in velocity occur to ensure proper physical modelling. This is achieved by using the finite accelerations and decelerations which accompany changes of motion state, rather than those associated with idealised, and physically impossible, step changes in velocity.

The pressure gradient at node point i is denoted as $\partial P_i/\partial s$, and the pressure at point 1 is P_1. The pressure at point j should be

$$P_i = P_1 + \frac{1}{2} \sum_{i=1}^{j-1} \left(\frac{\partial P_i}{\partial s} + \frac{\partial P_{i+1}}{\partial s} \right) \mathbf{s}_i \tag{52}$$

The resultant pressure force acting on the body is

$$\vec{\mathbf{F}} = -\frac{1}{2} \sum_{i=1}^{N} \left(P_i + P_{i+1}\right) s_i \vec{\mathbf{n}}_i \tag{53}$$

and the lift is

$$L = \frac{1}{2\left|\vec{\mathbf{U}}_\infty\right|} \sum_{i=1}^{N} \left(P_i + P_{i+1}\right) S_i \vec{\mathbf{s}}_i . \vec{\mathbf{U}}_\infty \tag{54}$$

The pressure moment about the reference point is

$$M_c = -\frac{1}{12} \sum_{i=1}^{N} \left[\left(2P_i + P_{i+1}\right) s_i \vec{\mathbf{s}}_i . \left(\vec{\mathbf{r}}_i - \vec{\mathbf{r}}_c\right) + \left(P_i + 2P_{i+1}\right) s_i \vec{\mathbf{s}}_i . \left(\vec{\mathbf{r}}_{i+1} - \vec{\mathbf{r}}_c\right) \right] \tag{55}$$

3.8 CALCULATION PROCEDURE

The calculation procedure for the model is illustrated in figure 7. At $t = 0$ there are no vortices in the wake - all vorticity is located within the control zone, and is determined by the boundary condition. The vorticity is discretised into vortices which are advanced during the time step Δt by application of the random walk and convection velocity contributions. By comparing the relative position of the vortices with that of the moving body, some are released into the wake but others remain within the control zone and are absorbed into the nascent layer according to their circulation and contribution to the boundary condition. The computation then advances by time step Δt.

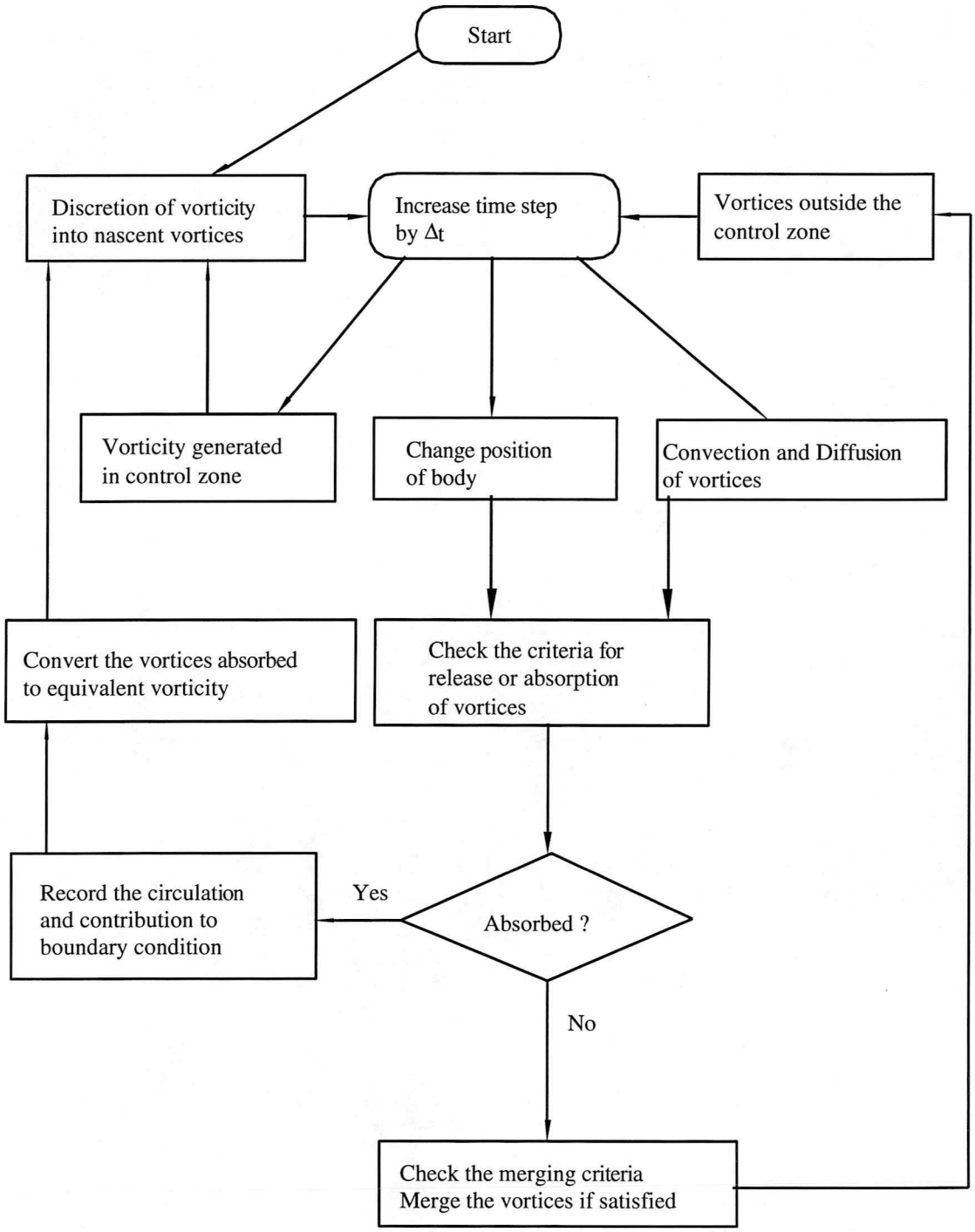

Figure 7: Diagram of calculation procedure

4 RESULTS

The model has been used to predict some separated flows. The results for starting flow around a NACA0015 undergoing various motions are presented below. The aerofoil cases include impulse starts at angles of attack 10° and 20°, ramp-up motion and ramp-up ramp-down triangle motion.

4.1 AEROFOIL UNSTEADY STATIC

Results for unsteady static flow around a NACA0015 undergoing impulse starts are presented in figures 8-11. Figures 8 and 9 are for $\alpha = 10°$ while figures 10 and 11 are for $\alpha = 20°$. For each case the time history of angle of attack, normal force coefficient, moment coefficient, and tangential force coefficient, together with the charts for C_n *vs* α, $C_{m1/4}$ *vs* α and C_t *vs* α, and vortex pattern are given.

For the case of $\alpha = 10°$, the C_n, $C_{m1/4}$, and C_t distributions, figure 8, illustrate the classic features of starting flow, i.e. an initial impulse followed by a gradual build up to steady state values corresponding to the increasing circulation which develops around the aerofoil. This process is further illustrated in figure 9 where the starting vortex can be seen to be carrying circulation downstream. The circulation around the body surface increases to maintain constancy of total circulation.

The situation for $\alpha = 20°$ is different. In figure 10 C_n overshoots soon after the impulse start and then undergoes a fluctuation around a lower average value. $C_{m1/4}$ and C_t exhibit similar trends. The associated vortex pattern, figure 11, illustrates the formation and discharge of the starting vortex and this corresponds to the initial behaviour of the aerodynamic forces. Subsequently, as separated flow develops over the upper surface, alternate vortex shedding begins corresponding to the start of the fluctuations in the aerodynamic forces. Vortex passage over the surface and dead air zones can be clearly identified in the pressure plots. The close correspondance between the shedding pattern and loadings is an encouraging feature of the method.

4.2 AEROFOIL RAMP-UP

Figures 12 and 13 show the results of the NACA0015 ramping from $-1°$ to $40°$ with a reduced frequency of 0.0487. Again, the time history of angle of attack, normal force coefficient, moment coefficient, and tangential force coefficient, together with the charts for C_n *vs* α, $C_{m1/4}$ *vs* α and C_t *vs* α, and the vortex pattern are presented. Both computational and experimental results are shown for comparison purposes. The level of agreement for this typical Reynolds number provides confidence in the applicability of the method to problems involving moving bodies. The delay in separation and increased maximum loads typical of dynamic stall are well predicted. The effect of vortex passage over the surface is illustrated by the additional increment in C_n and the large increase in the local suction on the upper surface. The normal force collapses after the vortex is shed from the aerofoil.

The model predicts an slightly earlier vortex induced increment of C_n and $C_{m1/4}$. This means that the vortices roll up earlier, and this might be due to the contribution of the vortex core function and the discretisation of the vorticity. The model also predicts a relatively smaller peak C_t with a less damped time history. These differences might be due to turbulent diffusion, which is not incorporate into the model.

4.3 AEROFOIL RAMP-UP and RAMP-DOWN

Figures 14 and 15 show the computational results for the NACA0015 during ramp up and down triangle motion. Again, the time history of angle of attack, normal force coefficient, moment coefficient, and tangential force coefficient, together with the charts for C_n *vs* α, $C_{m1/4}$ *vs* α

Aerofoil NACA 0015

Reynolds Number = 670000

Reduced Pitch Rate = 0.0

No of Panel = 80

No of Subpanel = 5

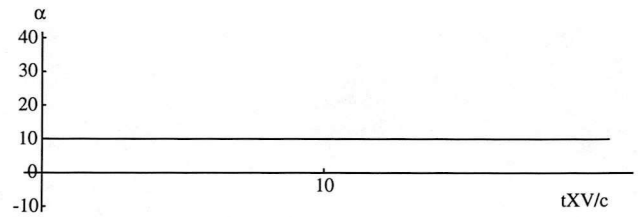

angle of attack

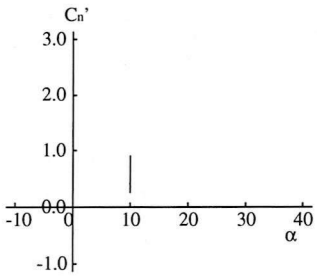

normal force coefficient

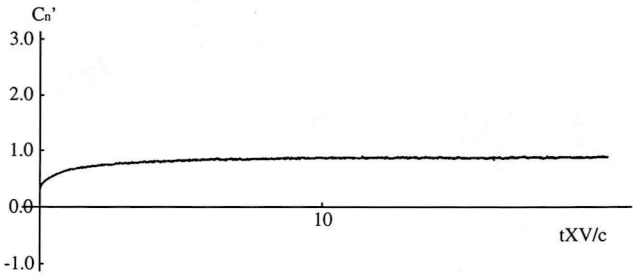

normal force coefficient

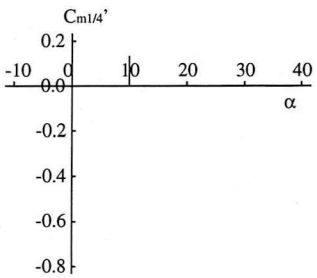

moment coefficient

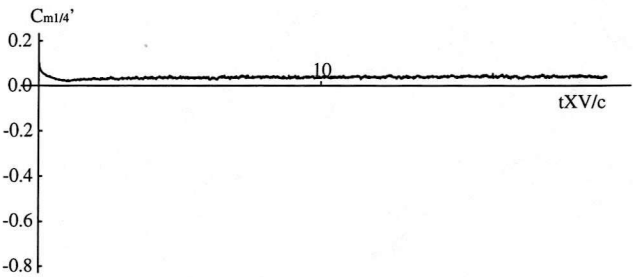

moment coefficient

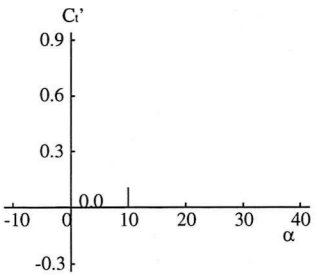

tangential force coefficient

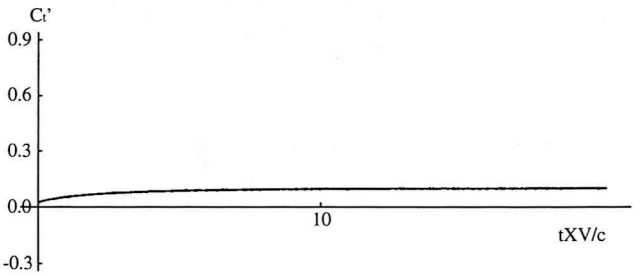

tangential force coefficient

Figure 8: Characteristics of the NACA0015 in impulsive flow at $\alpha = 10°$

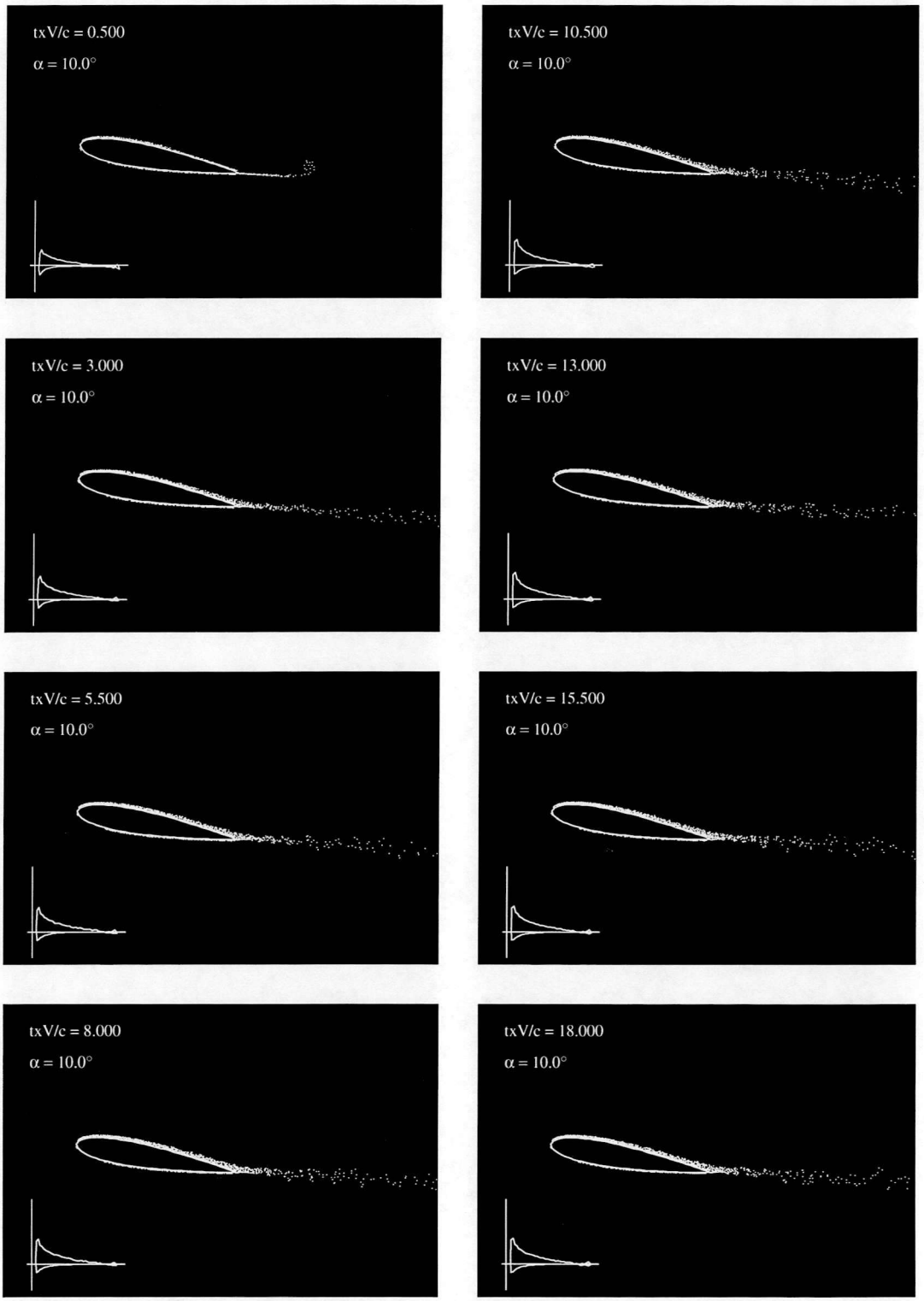

Aerofoil: NACA0015
Reynolds Number = 670000

No of Panel = 80
No of Subpanel = 5

Figure 9: Vortex pattern for the NACA0015 at $\alpha = 10°$

Aerofoil NACA 0015

Reynolds Number = 670000

Reduced Pitch Rate = 0.0

No of Panel = 80

No of Subpanel = 5

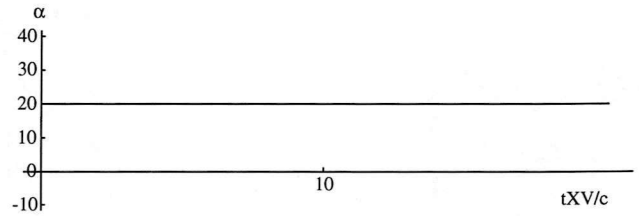

angle of attack

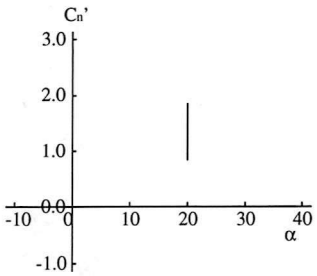

normal force coefficient

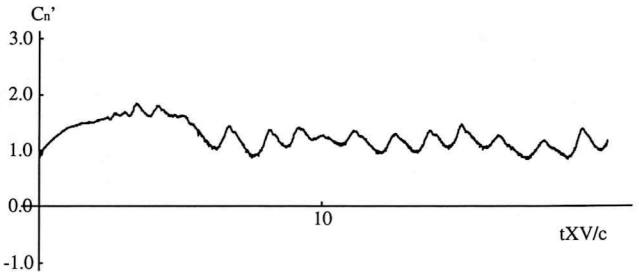

normal force coefficient

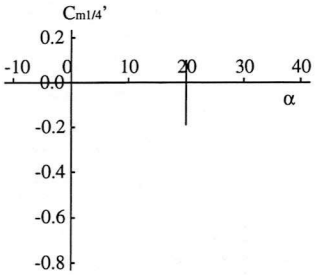

moment coefficient

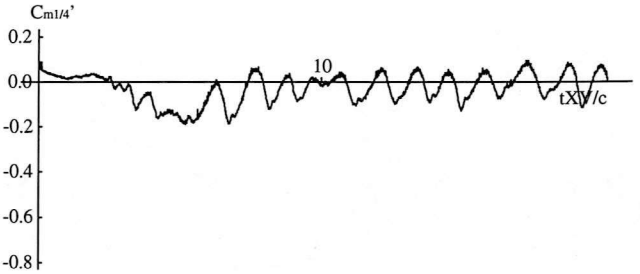

moment coefficient

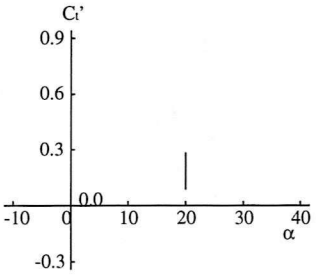

tangential force coefficient

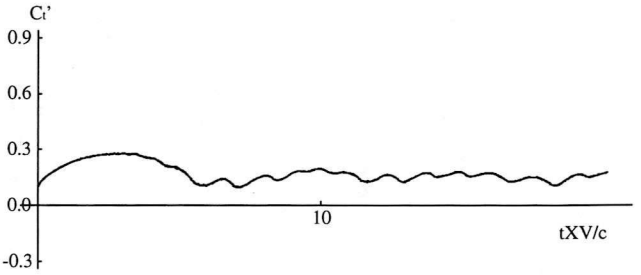

tangential force coefficient

Figure 10: Characteristics of the NACA0015 in impulsive flow at $\alpha = 20°$

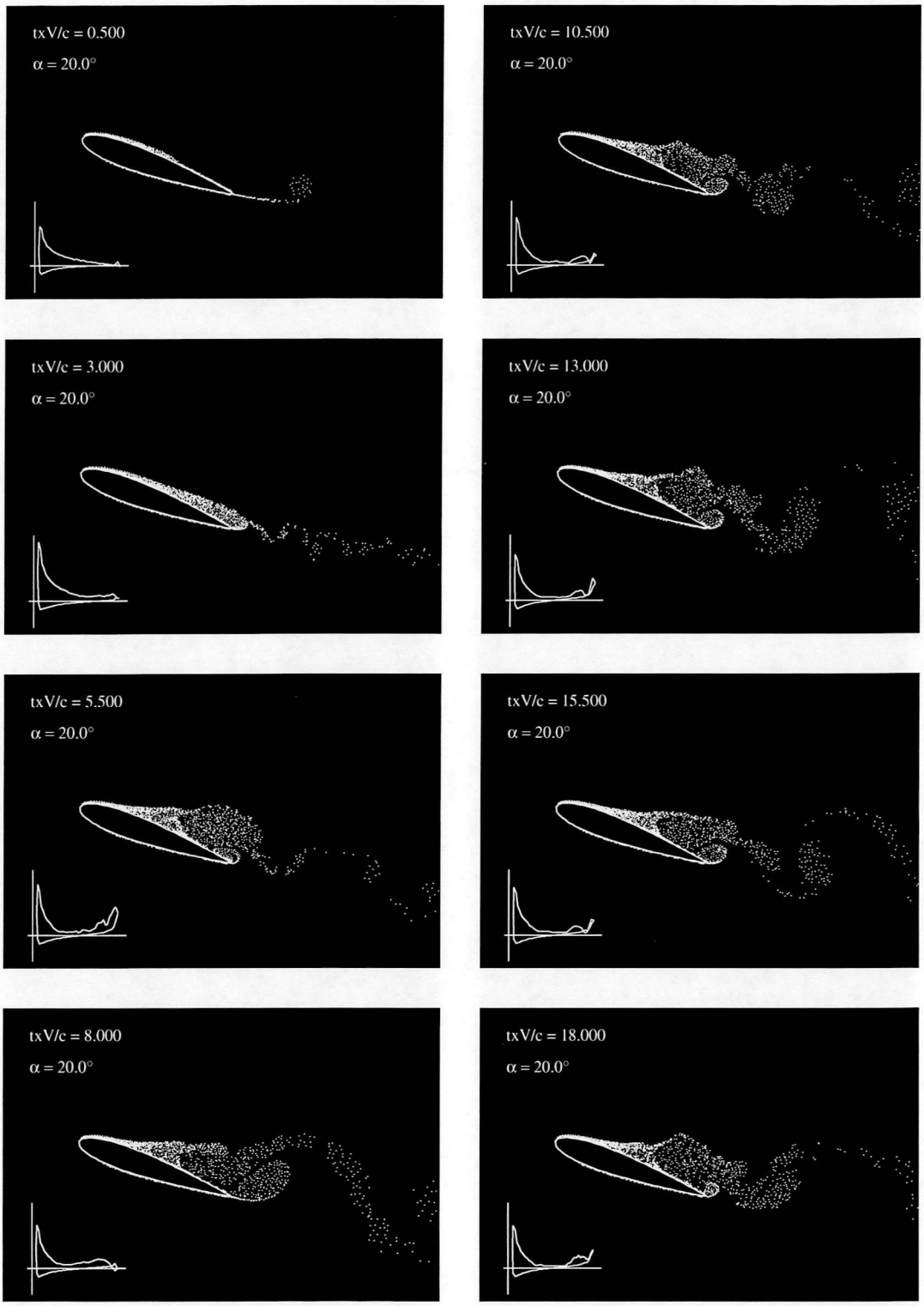

Aerofoil: NACA0015
Reynolds Number = 670000

No of Panel = 80
No of Subpanel = 5

Figure 11: Vortex pattern for the NACA0015 at $\alpha = 20°$

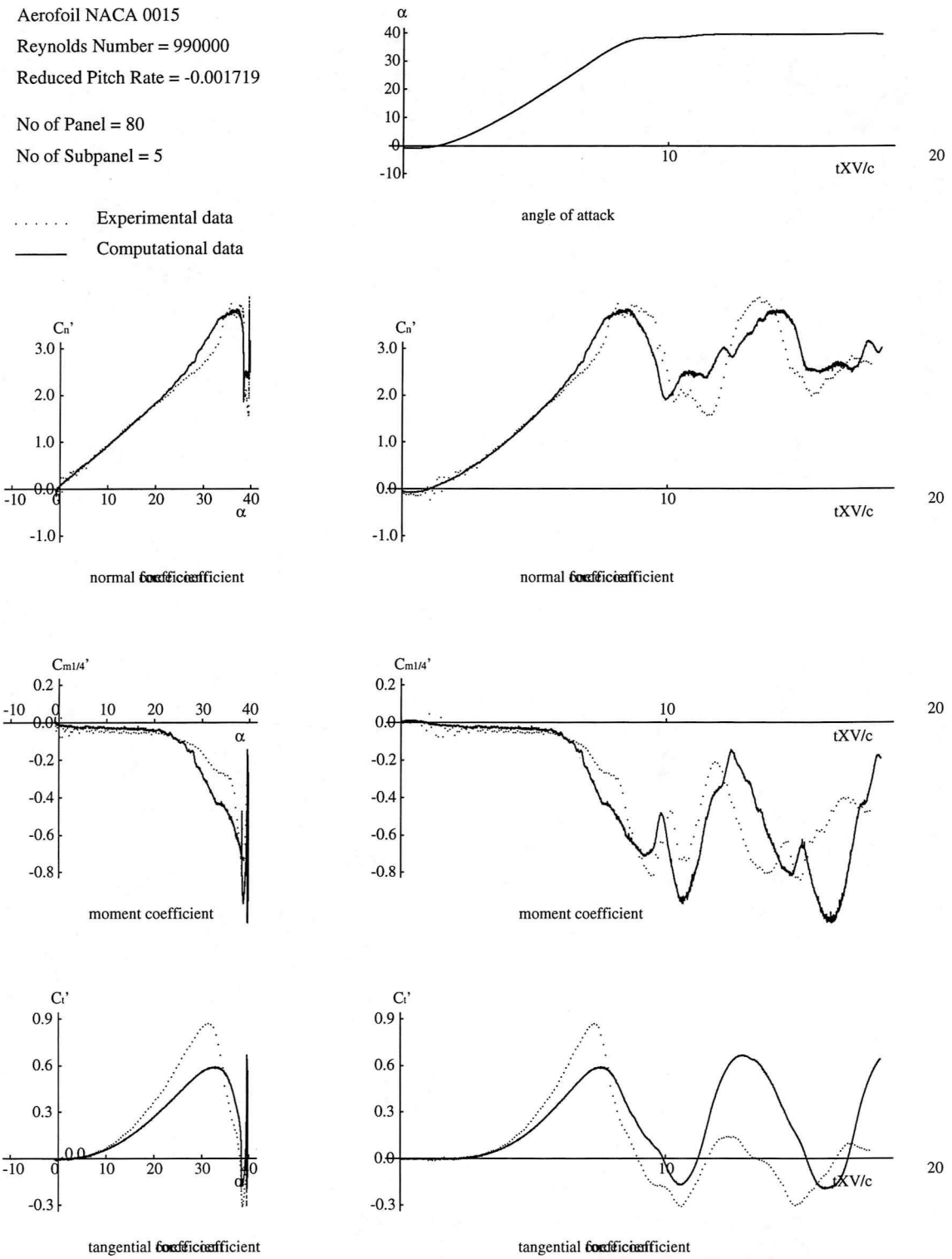

Figure 12: Characteristics of the NACA0015 during RAMP-UP

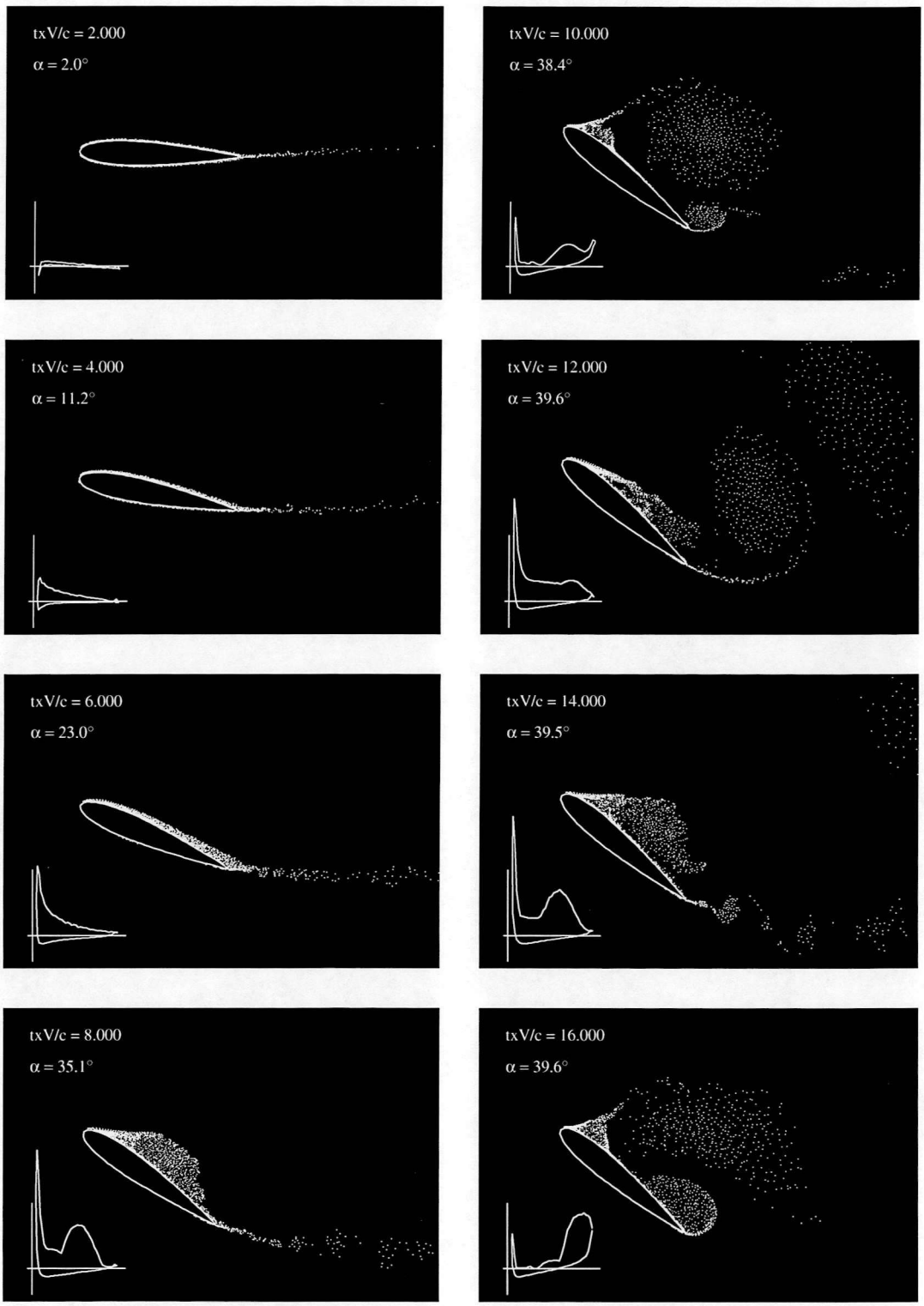

Aerofoil: NACA0015
Reynolds Number = 990000

Reduced Pitch Rate = 0.0487
No of Subpanel = 5

Figure 13: Vortex pattern for the NACA0015 during RAMP-UP

and C_t *vs* α, and vortex pattern are presented in figure 15. The characteristic hystereses in the aerodynamic loads is predicted. Of particular importance is the reduction in C_n during ramp down, especially the development of negative values at positive incidence, a feature which should cause concern to helicopter aerodynamicists. During ramp-up the processes are virtually identical to those described in the previous section. However the delay in reattachment and lack of vortex lift during ramp-down results in lower C_n values. Although upper surface suction starts to build up during ramp-down at higher incidence, this process is undermined by the continual reduction in incidence and possibly by the influence of the vortex system previously shed.

5 CONCLUSIONS

The following conclusions can be drawn at the present time:

1. A discrete vortex model has been developed which predicts separated, incompressible flows without the requirement for a boundary layer calculation or empirical specification of separation points. The control zone and multi-panel discretisation introduced in the paper make this prediction possible.

2. Despite the lack of some modelling features, e.g. turbulent diffusion, comparison between results from the model and experiments provides confidence in its capability to predict the dynamic stall and reattachment process on aerofoils, a task beyond the capability of most other models at present, and more general problems in incompressible aerodynamics.

6 REFERENCES

1. T. Sarpkaya, 1989, Computational Methods With Vortices - The 1988 Freeman Scholar Lecture

2. A. Leonard, 1985, Computing three-dimensional incompressible flows with vortex elements, Ann. Rev. Fluid Mech. 17, 523.

3. P.R. Spalart, A. Leonard & D. Baganoff, 1983, Numerical Simulation of Separated Flows, NASA TM 84328

4. P. R. Spalart, 1988, Vortex Methods for Separated Flows, NASA TM 100068

5. D.T.C. Porthouse & R.I. Lewis, 1981, Simulation of Viscous Diffusion for Extension of the Surface Vorticity Method to Boundary Layer and Separated Flows, Jour. Mech. Eng. Science. 23, 157-167

6. M. Vezza, 1992, A New Vortex Method for Modelling Two-Dimensional, Unsteady, Incompressible, Viscous Flows. G.U. Aero Report No. 9245.

7. H. J. Lugt, 1983, "Vortex Flow in Nature and Technology", John Wiley & Sons.

8. R.A.McD. Galbraith and F.N. Coton, A Review of Low Reynolds Number Aerodynamic Research at the University of Glasgow.

9. R.A.McD Galbraith, M.W. Gracey and E. Leitch, Contract Report for the Science and Engineering Research Coucil. G.U AERO report 9201.

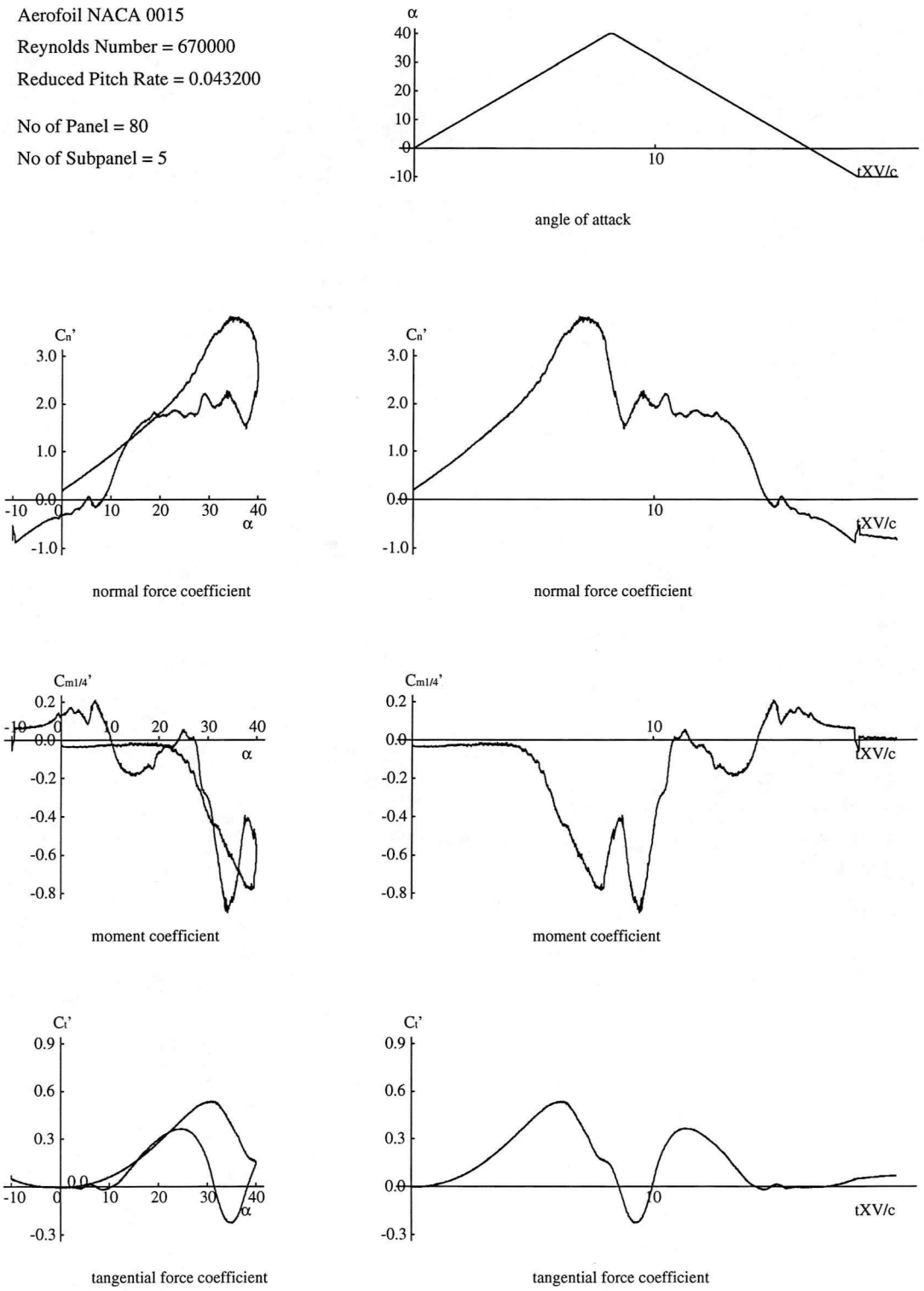

Figure 14: Characteristics of the NACA0015 during RAMP-UP RAMP-DOWN

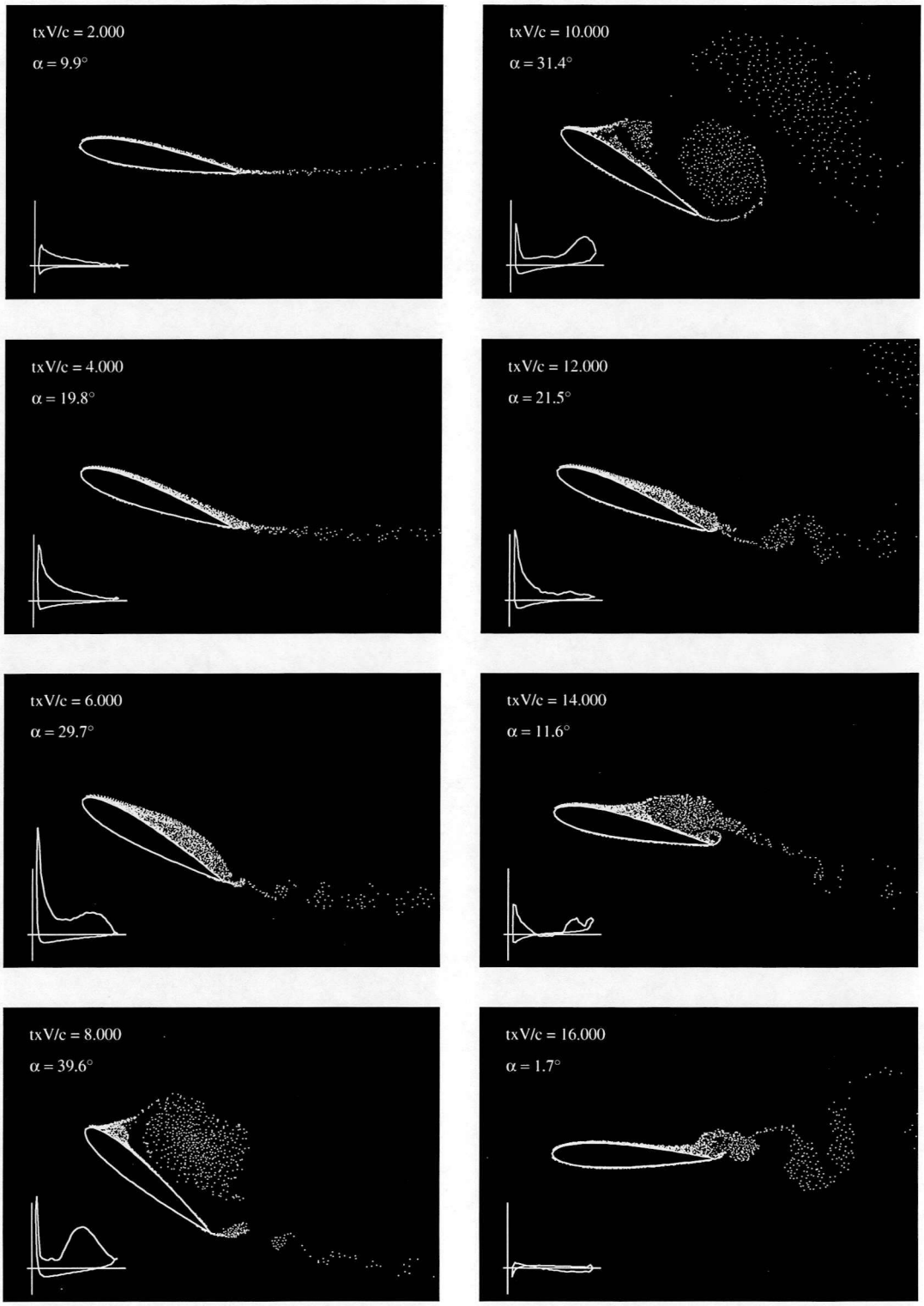

Figure 15: Vortex pattern for the NACA0015 during RAMP-UP RAMP-DOWN

A APPENDIX

The velocity of point $\mathbf{r}_p$ induced by vortex with circulation $d\Gamma$ at $\mathbf{r}$ is

$$d\vec{\mathbf{U}}_p = \vec{\mathbf{k}} \times \frac{(d\Gamma)(\vec{\mathbf{r}}_p - \vec{\mathbf{r}})}{2\pi \left\|\vec{\mathbf{r}}_p - \vec{\mathbf{r}}\right\|^2} = -\vec{\mathbf{k}} \times \frac{(d\Gamma)(\vec{\mathbf{r}} - \vec{\mathbf{r}}_p)}{2\pi \left\|\vec{\mathbf{r}} - \vec{\mathbf{r}}_p\right\|^2} \tag{56}$$

where

$$d\Gamma = 2\Omega_B dA$$

By integrating over the body area, the induced velocity becomes

$$\begin{aligned} \vec{\mathbf{U}}_p &= \int_{A_B} d\vec{\mathbf{U}}_p \\ &= -\frac{\Omega_B}{2\pi} \sum_m \vec{\mathbf{s}}_m \int_0^{\ell_m} \ln \left\|\vec{\mathbf{r}} - \vec{\mathbf{r}}_p\right\|^2 ds = -\frac{\Omega_B}{2\pi} \sum_m \vec{\mathbf{s}}_m \mathbf{I}_1 \end{aligned} \tag{57}$$

where

$$\begin{aligned} \mathbf{I}_1 &= \int_0^{\ell_m} \ln \left\|\vec{\mathbf{r}} - \vec{\mathbf{r}}_p\right\|^2 ds_m \\ &= \ell_m \ln c_1 + \frac{b_0}{\ell_m} \ln\left(\frac{c_1}{a_0}\right) + \frac{2c_0}{\ell_m}\left[\tan^{-1}\left(\frac{c_2}{c_0}\right) - \tan^{-1}\left(\frac{b_0}{c_0}\right)\right] - 2\ell_m \end{aligned}$$

and

$$\begin{aligned} b_0 &= \triangle x_{mp} \triangle x_m + \triangle y_{mp} \triangle y_m \\ c_0 &= \triangle x_{mp} \triangle y_m - \triangle y_{mp} \triangle x_m \\ c_1 &= \triangle x_{m+1p}^2 + \triangle y_{m+1p}^2 \\ c_2 &= \triangle x_{m+1p} \triangle x_m + \triangle y_{m+1p} \triangle y_m \end{aligned}$$

$$\begin{aligned} F_{ji} &= \int_0^{\ell_j} \vec{\mathbf{U}}_p . \vec{\mathbf{n}} ds_j \\ &= -\frac{\Omega_B}{2\pi} \int_0^{\ell_j} \left(\int_{S_B} \vec{\mathbf{s}} \ln \left\|\vec{\mathbf{r}} - \vec{\mathbf{r}}_p\right\|^2 ds \right) . \vec{\mathbf{n}} ds_j \\ &= -\frac{\Omega_B}{2\pi} \sum_m (\vec{\mathbf{s}}_m . \vec{\mathbf{n}}_j)\, \mathbf{I}_2 \end{aligned} \tag{58}$$

$$\mathbf{I}_2 = \int_0^{\ell_j} \int_0^{\ell_m} \ln \left\|\vec{\mathbf{r}} - vec\mathbf{r}_p\right\|^2 ds_m ds_j$$

$$\begin{aligned} \mathbf{I}_2 &= \ell_m \ell_j \ln c_3 - 3\ell_m \ell_j + \frac{(b_3 a_1 - 2a_5 b_1)}{2\ell_j \ell_m} \ln\left(\frac{c_3}{a_1}\right) \\ &+ \frac{(2a_4 b_1 - b_4 a_1)}{\ell_j \ell_m}\left[\tan^{-1}\left(\frac{-b_1 + \ell_j^2}{c_4}\right) - \tan^{-1}\left(\frac{b_1}{c_4}\right)\right] \\ &+ \frac{(2a_3 - b_3)\,\ell_j}{2\ell_m} \ln\left(\frac{c_3}{c_6}\right) + \frac{(2a_4 - b_4)\,\ell_j}{\ell_m}\left[\tan^{-1}\left(\frac{c_9}{c_{11}}\right) - \tan^{-1}\left(\frac{c_{10}}{c_{11}}\right)\right] \\ &+ \frac{(-b_3 a_2 + 2a_3 b_2)}{2\ell_j \ell_m} \ln\left(\frac{c_6}{a_2}\right) + \frac{(-2a_4 b_2 + b_4 a_2)}{\ell_j \ell_m}\left[\tan^{-1}\left(\frac{-b_2 + \ell_j^2}{c_7}\right) - \tan^{-1}\left(\frac{b_2}{c_7}\right)\right] \end{aligned}$$

for $|m-j|>1$,

$$\mathbf{I}_2 = \ell_j^2\left(2\ln\ell_j - 3\right)$$

for $m=j$,

$$\begin{aligned}
\mathbf{I}_2 &= -3\ell_{j+1}\ell_j + \frac{a_6\ell_j}{\ell_{j+1}}\left[\tan^{-1}\left(\frac{a_3+\ell_{j+1}^2}{a_6}\right) - \tan^{-1}\left(\frac{a_3}{a_6}\right)\right] \\
&+ \frac{2a_6^3}{\ell_j^3\ell_{j+1}}\left[\tan^{-1}\left(\frac{a_3+\ell_j^2}{a_6}\right) - \tan^{-1}\left(\frac{a_3}{a_6}\right)\right] \\
&+ \frac{a_6\left(a_6^2-a_3^2\right)}{\ell_j^3\ell_{j+1}}\left[\tan^{-1}\left(\frac{a_6}{a_3+\ell_j^2}\right) - \tan^{-1}\left(\frac{a_6}{a_3}\right)\right] \\
&+ \frac{a_3\ell_{j+1}}{2\ell_j}\ln\left[\frac{\ell_{j+1}^2+2a_3+\ell_j^2}{\ell_{j+1}^2}\right] + \frac{a_3\ell_j}{2\ell_{j+1}}\ln\left[\frac{\ell_{j+1}^2+2a_3+\ell_j^2}{\ell_j^2}\right] \\
&+ \ell_j\ell_{j+1}\ln\left(\ell_{j+1}^2+2a_3+\ell_j^2\right)
\end{aligned}$$

for $m=j+1$, and

$$\begin{aligned}
\mathbf{I}_2 &= -3\ell_{j-1}\ell_j + \frac{b_6\ell_j}{\ell_{j-1}}\left[\tan^{-1}\left(\frac{b_3+\ell_{j-1}^2}{b_6}\right) - \tan^{-1}\left(\frac{b_3}{b_6}\right)\right] \\
&+ \frac{2b_6^3}{\ell_j^3\ell_{j-1}}\left[\tan^{-1}\left(\frac{b_3+\ell_j^2}{b_6}\right) - \tan^{-1}\left(\frac{b_3}{b_6}\right)\right] \\
&+ \frac{b_6\left(b_6^2-b_3^2\right)}{\ell_j^3\ell_{j-1}}\left[\tan^{-1}\left(\frac{b_6}{b_3+\ell_j^2}\right) - \tan^{-1}\left(\frac{b_6}{b_3}\right)\right] \\
&+ \frac{b_3\ell_{j-1}}{2\ell_j}\ln\left[\frac{\ell_{j-1}^2+2b_3+\ell_j^2}{\ell_{j-1}^2}\right] + \frac{b_3\ell_j}{2\ell_{j-1}}\ln\left[\frac{\ell_{j-1}^2+2b_3+\ell_j^2}{\ell_j^2}\right] \\
&+ \ell_j\ell_{j-1}\ln\left(\ell_{j-1}^2+2b_3+\ell_j^2\right)
\end{aligned}$$

for $m=j-1$.

Some variables are expressed as

$$\begin{aligned}
a_1 &= \triangle x_{m+1j}^2 + \triangle y_{m+1j}^2 \\
a_2 &= \triangle x_{mj}^2 + \triangle y_{mj}^2 \\
a_3 &= \triangle x_{mj}\triangle x_m + \triangle y_{mj}\triangle y_m \\
a_4 &= \triangle x_{mj}\triangle y_m - \triangle y_{mj}\triangle x_m \\
a_5 &= \triangle x_{m+1j}\triangle x_m + \triangle y_{m+1j}\triangle y_m \\
a_6 &= \sqrt{\ell_j^2\ell_{j+1}^2 - a_3^2} \\
b_1 &= \triangle x_{m+1j}\triangle x_j + \triangle y_{m+1j}\triangle y_j \\
b_2 &= \triangle x_{mj}\triangle x_j + \triangle y_{mj}\triangle y_j \\
b_3 &= \triangle x_m\triangle x_j + \triangle y_m\triangle y_j \\
b_4 &= \triangle x_j\triangle y_m - \triangle y_j\triangle x_m \\
b_6 &= \sqrt{\ell_j^2\ell_{j-1}^2 - b_3^2} \\
c_3 &= \triangle x_{m+1j+1}^2 + \triangle y_{m+1j+1}^2
\end{aligned}$$

$$
\begin{aligned}
c_4 &= \triangle x_{m+1j} \triangle y_j - \triangle y_{m+1j} \triangle x_j \\
c_6 &= \triangle x^2_{mj+1} + \triangle y^2_{mj+1} \\
c_7 &= \triangle x_{mj} \triangle y_j - \triangle y_{mj} \triangle x_j \\
c_9 &= \triangle x_{m+1j+1} \triangle x_m + \triangle y_{m+1j+1} \triangle y_m \\
c_{10} &= \triangle x_{mj+1} \triangle x_m + \triangle y_{mj+1} \triangle y_m \\
c_{11} &= \triangle x_{mj+1} \triangle y_m - \triangle y_{mj+1} \triangle x_m
\end{aligned}
$$